substructural elements found in many small molecules (*13*), developing better methods for iteratively coupling those building blocks together, and advancing the capacity for biosynthesis-inspired cyclizations of linear precursors to yield complex natural product frameworks. Achieving these objectives stands to better enable the scientific community to bring the substantial power of small-molecule synthesis to bear upon many important unsolved problems in society.

REFERENCES AND NOTES

1. R. B. Merrifield, *Science* **150**, 178–185 (1965).
2. M. H. Caruthers, *Science* **230**, 281–285 (1985).
3. O. J. Plante, E. R. Palmacci, P. H. Seeberger, *Science* **291**, 1523–1527 (2001).
4. S. V. Ley, D. E. Fitzpatrick, R. J. Ingham, R. M. Myers, *Angew. Chem. Int. Ed.* **54**, 10.1002/anie.201410744 (2015).
5. S. Fuse, K. Machida, T. Takahashi, in *New Strategies in Chemical Synthesis and Catalysis*, B. Pignataro, Ed. (Wiley, Weinheim, Germany, 2012), chap. 2.
6. A. G. Godfrey, T. Masquelin, H. Hemmerle, *Drug Discov. Today* **18**, 795–802 (2013).
7. S. Newton *et al*., *Angew. Chem. Int. Ed.* **53**, 4915–4920 (2014).
8. P. M. Dewick, *Medicinal Natural Products: A Biosynthetic Approach* (Wiley, West Sussex, UK, 2009).
9. E. Vitaku, D. T. Smith, J. T. Njardarson, *J. Med. Chem.* **57**, 10257–10274 (2014).
10. R. A. Yoder, J. N. Johnston, *Chem. Rev.* **105**, 4730–4756 (2005).
11. E. M. Stocking, R. M. Williams, *Angew. Chem. Int. Ed.* **42**, 3078–3115 (2003).
12. F. Kopp, M. A. Marahiel, *Nat. Prod. Rep.* **24**, 735–749 (2007).
13. E. M. Woerly, J. Roy, M. D. Burke, *Nat. Chem.* **6**, 484–491 (2014).
14. E. P. Gillis, M. D. Burke, *J. Am. Chem. Soc.* **129**, 6716–6717 (2007).
15. N. Miyaura, A. Suzuki, *Chem. Rev.* **95**, 2457–2483 (1995).
16. E. P. Gillis, M. D. Burke, *Aldrichim Acta* **42**, 17–27 (2009).
17. E. M. Woerly, A. H. Cherney, E. K. Davis, M. D. Burke, *J. Am. Chem. Soc.* **132**, 6941–6943 (2010).
18. K. C. Gray *et al*., *Proc. Natl. Acad. Sci. U.S.A.* **109**, 2234–2239 (2012).
19. K. Fujita, R. Matsui, T. Suzuki, S. Kobayashi, *Angew. Chem. Int. Ed.* **51**, 7271–7274 (2012).
20. C. H. Heathcock, S. Piettre, R. B. Ruggeri, J. A. Ragan, J. C. Kath, *J. Org. Chem.* **57**, 2554–2566 (1992).
21. E. L. Elliott, C. R. Ray, S. Kraft, J. R. Atkins, J. S. Moore, *J. Org. Chem.* **71**, 5282–5290 (2006).
22. M. Mentel, R. Breinbauer, *Top. Curr. Chem.* **278**, 209–241 (2007).
23. S. Maechling, J. Good, S. D. Lindell, *J. Comb. Chem.* **12**, 818–821 (2010).
24. Materials and methods are available as supplementary materials on *Science* Online.
25. T. Kinzel, Y. Zhang, S. L. Buchwald, *J. Am. Chem. Soc.* **132**, 14073–14075 (2010).
26. E. P. Gillis, M. D. Burke, *J. Am. Chem. Soc.* **130**, 14084–14085 (2008).
27. J. E. Grob *et al*., *Org. Lett.* **14**, 5578–5581 (2012).
28. D. G. Hall, Ed., *Boronic Acids: Preparation and Applications in Organic Synthesis, Medicine and Materials* (Wiley, Weinheim, Germany, 2011).
29. F. Bracher, B. Schulte, *Nat. Prod. Res.* **17**, 293–299 (2003).
30. T. K. M. Shing, J. Yang, *J. Org. Chem.* **60**, 5785–5789 (1995).
31. E. J. Corey, L. Kürti, in *Enantioselective Chemical Synthesis: Methods, Logic, and Practice* (Direct Book Publishing, Dallas, TX, 2010), pp. 121–151.
32. R. M. Wilson, W. S. Jen, D. W. C. Macmillan, *J. Am. Chem. Soc.* **127**, 11616–11617 (2005).
33. S. A. Snyder, D. S. Treitler, A. Schall, *Tetrahedron* **66**, 4796–4804 (2010).

ACKNOWLEDGMENTS

We acknowledge the NIH (grants GM080436 and GM090153), the NSF (grant 0747778), HHMI, and Bristol-Myers Squibb for funding. M.D.B. is an HHMI Early Career Scientist, J.L. was an HHMI International Student Research Fellow, and J.L. and E.P.G. were Bristol-Myers Squibb Graduate Fellows. We thank D. Gray for performing the x-ray analysis on **N-bromoacyl-14**. The University of Illinois has filed patent applications on MIDA boronate chemistry and the automated synthesis platform reported herein. These inventions have been licensed to REVOLUTION Medicines, a company for which M.D.B. is a founder. Metrical parameters for the structure of **N-bromoacyl-14** are available free of charge from the Cambridge Cyrstallographic Data Centre under reference CCDC-1045844.

SUPPLEMENTARY MATERIALS

www.sciencemag.org/content/347/6227/1221/suppl/DC1
Materials and Methods
Supplementary Text
Figs. S1 to S14
Tables S1 to S3
References (*34*–*52*)

22 December 2014; accepted 12 February 2015
10.1126/science.aaa5414

LUNAR GEOLOGY

A young multilayered terrane of the northern Mare Imbrium revealed by Chang'E-3 mission

Long Xiao,[1,2]* Peimin Zhu,[1]* Guangyou Fang,[3]* Zhiyong Xiao,[1,4] Yongliao Zou,[5] Jiannan Zhao,[1] Na Zhao,[1] Yuefeng Yuan,[1] Le Qiao,[1] Xiaoping Zhang,[2] Hao Zhang,[1] Jiang Wang,[1] Jun Huang,[1] Qian Huang,[1] Qi He,[1] Bin Zhou,[3] Yicai Ji,[3] Qunying Zhang,[3] Shaoxiang Shen,[3] Yuxi Li,[3] Yunze Gao[3]

China's Chang'E-3 (CE-3) spacecraft touched down on the northern Mare Imbrium of the lunar nearside (340.49°E, 44.12°N), a region not directly sampled before. We report preliminary results with data from the CE-3 lander descent camera and from the Yutu rover's camera and penetrating radar. After the landing at a young 450-meter crater rim, the Yutu rover drove 114 meters on the ejecta blanket and photographed the rough surface and the excavated boulders. The boulder contains a substantial amount of crystals, which are most likely plagioclase and/or other mafic silicate mineral aggregates similar to terrestrial dolerite. The Lunar Penetrating Radar detection and integrated geological interpretation have identified more than nine subsurface layers, suggesting that this region has experienced complex geological processes since the Imbrian and is compositionally distinct from the Apollo and Luna landing sites.

Chang'E-3 (CE-3) landed at 340.49°E, 44.12°N on the Moon on 14 December 2013, and it released the Yutu (Jade Rabbit) rover the next morning (*1*). This was the first soft landing on the Moon since the Soviet Union's Luna 24 mission in 1976 and is a new landing site in the north part of the Mare Imbrium (fig. S1). Yutu is China's first lunar geologic mission and traveled in total ~114 m on the lunar surface. Following a zigzagging route, Yutu came to a halt about 20 m to the southwest of the landing site (Fig. 1). Yutu explored the lunar surface and subsurface near a young crater (fig. S2) using its four main instruments: Panoramic Camera, Lunar Penetrating Radar (LPR), Visible–Near Infrared Spectrometer (VNIS), and Active Particle-Induced X-ray Spectrometer (APXS). In this study, we report the preliminary results obtained from the cameras and LPR.

[1]China University of Geosciences, Wuhan 430074, China. [2]Macau University of Science and Technology, Macau, China. [3]Institute of Electronics, China Academy of Science, Beijing 100190, China. [4]The Centre for Earth Evolution and Dynamics, University of Oslo, Sem Sælandsvei 24, 0371 Oslo, Norway. [5]National Astronomical Observatories, China Academy of Science, Beijing 100012, China.
***Corresponding author. E-mail: longxiao@cug.edu.cn (L.X.); zhupm@cug.edu.cn (P.Z.); gyfang@mail.ie.ac.cn (G.F.)**

High-resolution images returned by both Yutu and the lander show that the landing site features thin regolith and numerous small craters that are centimeters to tens of meters in diameter (Fig. 1 and figs. S3 to S6). Although at the regional scale the mare surface at the landing site appears relatively flat, the landing site is located ~50 m from the eastern rim of the ~450-m crater (C_1) (*2*). The traversed area of the Yutu rover was wholly restricted within the continuous ejecta deposits (fig. S2). Crater size-frequency distribution measurements (*2*) for the continuous ejecta deposits of the C_1 crater yield a minimum model age of ~27 million years (My) and a maximum model age of ~80 My, which is late Copernican (*3*), consistent with the estimation made from the preservation state of the crater and from the meter-sized boulders observed on the crater rim (*2*).

Yutu drove very close to the rim of the C_1 crater, and its panoramic cameras photographed the shape and interior features of the crater. A full image of the crater was also acquired (fig. S4A) when Yutu stood behind the Loong rock (position number 13 in Fig. 1) (*1*). This circular-rimmed crater has distinct rocky walls and rims, except on the northern side. The ejected boulders are

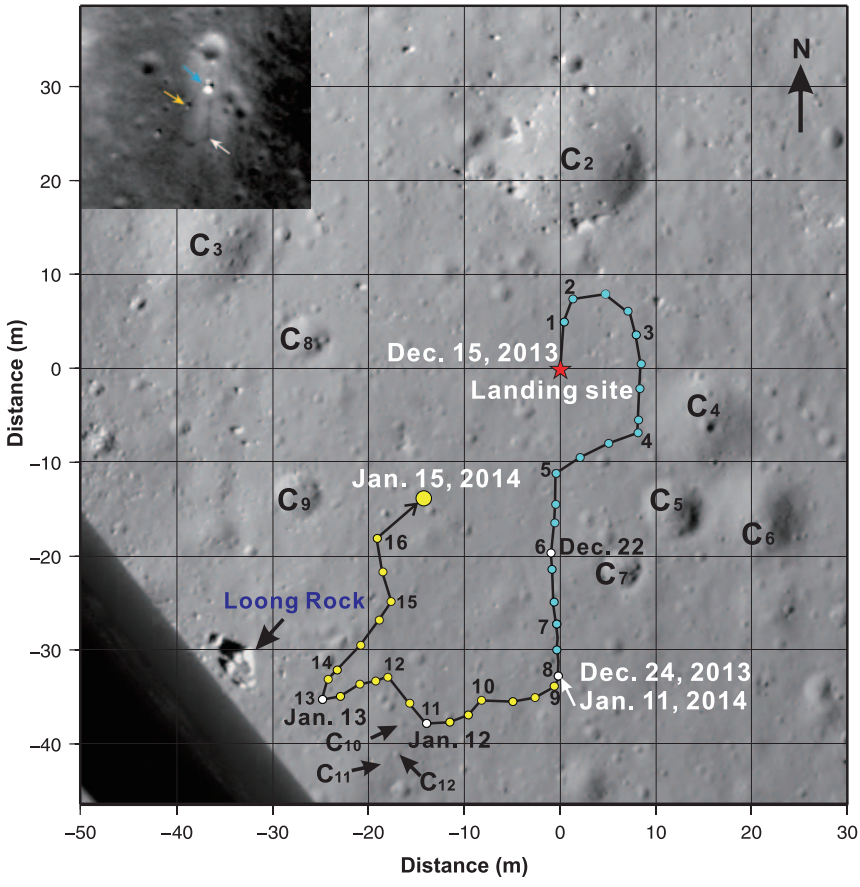


Fig. 1. Yutu's path on the Moon. The cyan and yellow dots mark the first and second lunar daytime stops, which ended on 24 December 2013 and 15 January 2014, respectively. The numbers aligned to the dots denote the positions where the LPR was rebooted. The white dots indicate positions where the APXS, VNIS, and panoramic camera gathered data. The context image was taken by the descent camera at an elevation of ~120 m, and the lower left corner was blocked by the lander. The inset image shows the positions of the CE-3 lander (blue arrow), the Yutu rover (yellow arrow), and its track (dark gray line) (the white arrow points to the spot where Yutu rested for the first lunar night). The inset image was taken by the Lunar Reconnaissance Orbiter Camera Narrow Angle Camera (LROC NAC; NASA/Goddard/Arizona State University).

irregular in shape and of various sizes, which are up to several meters tall and wide—e.g., the Loong rock (~4 m long by ~1.5 m high).

Small craters on the ejecta blanket of the C_1 crater vary in shape, roughness, and albedo (fig. S4). Regolith exhumed by Yutu's wheels has a lower reflectance compared with regolith on the surface, which is probably due to larger grain sizes of regolith at depths (fig. S5). Extensive shallow and linear features are visible around the landing site (figs. S5 and S6). Most of them occur in two preferential directions and are intersected and/or cross-cut with each other (figs. S5 and S6). Although this region was affected by the recoil rockets during the landing process, as evident from the inset image shown in Fig. 1, any rocket jets would have formed continuous, multidirectional and/or radial features on the surface, which are not observed along the track of the Yutu rover. Furthermore, newly created surface features on the Moon should have a rougher appearance and display distinctively lower albedos compared with the surroundings, which are not observed at the landing site either. Nearby impact craters may also distribute radial ejecta rays to the surroundings, but their potential in forming such multigroup subparallel linear features is low. Alternatively, linear features with comparable scales and similar appearances were widely observed at the Apollo 11, 12, and 15 landing sites, which were interpreted to be caused by a combination of obliquely incident sunlight and small surface topographic irregularities (*4*, *5*). The linear features observed at the CE-3 landing site, therefore, could simply be illumination features caused by the undulated surface.

Orbital chemical composition measurements from the gamma ray spectrometer onboard Lunar Prospector revealed that this area may be covered by intermediate Ti mare basalts [$TiO_2 = 5 \pm 1$ weight percent (wt %) and FeO = 20 ± 2 wt %] (*6*). The Loong rock appears to be homogeneous in high-resolution images obtained by the Yutu rover (fig. S7). Coarse granular or porphyritic textures are visible within the boulder. The light-colored crystals are ~1.5 to 2 cm in length and exhibit diffuse margins (fig. S7B). Image comparisons between this outcrop and the Lunar Sample Compendium (http://curator.jsc.nasa.gov/lunar/lsc) indicate that the Loong rock is distinct in texture from the other lunar basalts or breccias. The light-colored crystals are most likely plagioclases or aggregates of plagioclase (*7*) and other mafic silicate minerals—e.g., pyroxene and olivine (*8*)—indicating that this boulder may be coarse-crystalline basalt or dolerite excavated by the impact that formed the C_1 crater.

The LPR onboard Yutu consists of two types of antennas that have different frequencies, allowing subsurface structures at the landing site to be resolved at different depths and vertical resolutions (*2*, *9*, *10*). The dominant frequencies of these two channels are 60 MHz (Channel 1) and 500 MHz (Channel 2). The LPR has obtained radar echoes along the whole traverse of Yutu. Here, we report the preliminary interpretations on the radar data returned from the two antennas.

The LPR data have been processed using a standard calibration method (*2*, *9*, *10*). The Channel 1 radar reveals subsurface structures to depths of ~400 m and resolves several interfaces that have clear reflection characteristics (Fig. 2B). Subsurface structures less than ~20 m deep are not well resolved by the Channel 1 radar because of both the lower resolution and signal-to-noise ratio caused by signal saturation at such small depths (*2*, *10*). The Channel 2B data, however, reveal structures at depths less than 12 m but with greater detail compared with the Channel 1 data (Fig. 2A).

The Yutu rover surveyed a small area over the Eratosthenian basalts within the Imbrium basin. These mare basalts are believed to be among the youngest [~2.5 billion years (Gy) old] (*11*), compared with the landing sites of Apollo and Luna missions (*3*). The uppermost and also the youngest stratigraphic unit at the landing site is a regolith layer formed from the ejecta deposits excavated in the formation of the C_1 crater (layer a in Fig. 2A). This layer is ~1 m thick, as inferred from the morphology of small craters at the landing site [(*2*) and fig. S3]. At different locations along Yutu's track, small

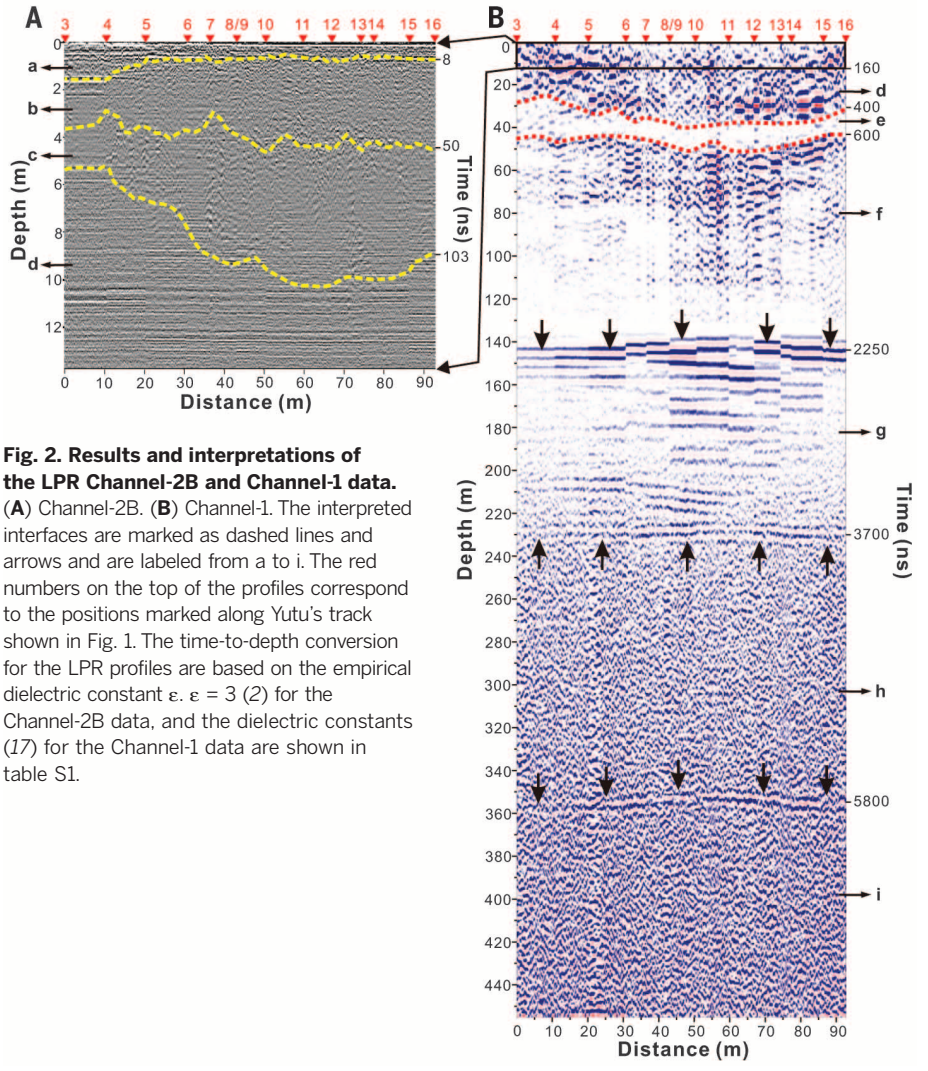


Fig. 2. Results and interpretations of the LPR Channel-2B and Channel-1 data. (**A**) Channel-2B. (**B**) Channel-1. The interpreted interfaces are marked as dashed lines and arrows and are labeled from a to i. The red numbers on the top of the profiles correspond to the positions marked along Yutu's track shown in Fig. 1. The time-to-depth conversion for the LPR profiles are based on the empirical dielectric constant ε. ε = 3 (*2*) for the Channel-2B data, and the dielectric constants (*17*) for the Channel-1 data are shown in table S1.

craters postdating the C_1 crater, such as the C_2 and C_4 craters (Fig. 1), have modified the local regolith thickness by impact excavation and deposition. This thickness variation is also resolved in the interpreted layer a from the Channel 2B data, which is ~2 m thick between positions 3 and 4 and ~1 m thick at the rest area along Yutu's track (Fig. 2A). Below the surface regolith layer are the remnant ejecta deposits from the C_1 crater, which are generally thicker near the crater rim and then thin outwardly (*12*). This layer of ~1 to ~4 m is recognized in the Channel 2B data (layer b in Fig. 2A), which is thicker from positions 4 to 16 (Fig. 1). Also, there may be many rocks with the size of about 0.3 to 1 m within the ejecta deposits, based on the presence of diffraction events of radar wave (see fig. S14).

Before the C_1 crater formed ~27 to 80 million years ago (Ma), a boulder-bearing paleoregolith layer (c in Fig. 2A) had accumulated at the base of the Eratosthenian basalts [~2.5 billion years ago (Ga)] by space weathering and impact gardening. Continuous ejecta from the C_1 crater was then deposited (layer b in Fig. 2A) over this paleoregolith layer. This layer is consistent with the third layer recognized at depths from ~4 to ~10 m from the Channel 2B (layer c in Fig. 2A). It exhibits a wide range of thickness from ~2 to ~6 m, which is consistent with the large variety of regolith depth over small distances on the Moon (*13*). It may be a record of the nonuniform production rate of regolith over the lunar surface and/or the disturbance by later impacts, such as the C_1 crater. Materials at depths larger than ~6 to 10 m (layer d in Fig. 2A) show regular layering and the radar echoes indicating larger density compared with shallower regolith or fractured ejecta deposits. These radar features suggest that layer d is made of thick competent rocks, most likely

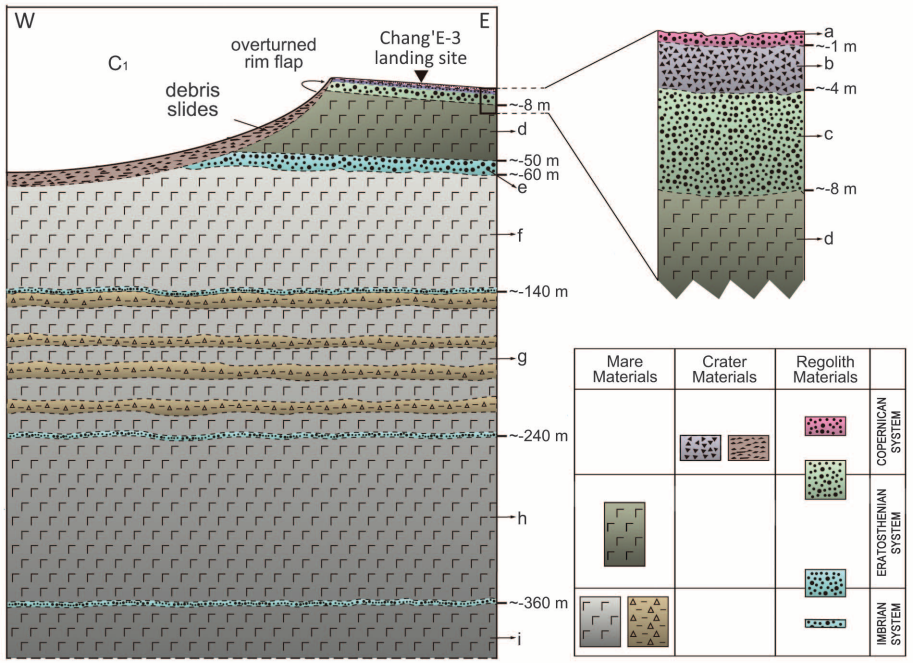


Fig. 3. Sketched geological cross section and an inferred profile of the CE-3 landing site. Yutu has detected seven subsurface interfaces, which formed from Imbrian to Copernican. Letters a to i indicate interpreted subsurface layers based on LPR data (Fig. 2).

similar to the Eratosthenian basalts beneath the paleoregolith layer.

The Channel 1 data reveal that the Eratosthenian basalts at the landing site extend to a depth of ~35 m (layer d in Fig. 2, A and B), which is consistent with the depth estimated from nearby impact craters that have excavated deeper Imbrian materials (*14*). Two clear interfaces that feature higher radar reflection strengths are shown at depths ~35 m and ~50 m (layer e in Fig. 2B), respectively. This fifth layer (layer e), is interpreted to be the paleoregolith formed on top of the Imbrian lava flows (>~3.3 Ga) (*11*), over which the Eratosthenian basalts were emplaced subsequently. A deeper layer between ~50 and 140 m has similar radar reflections to the Eratosthenian basalts resolved in layer d, suggesting that this layer probably represents the latest Imbrian basalts that filled in the Imbrium basin around 3.3 Ga (layer f in Fig. 2B). Other subhorizontal interfaces are visible at depths larger than ~140 m, such as those at depths of ~240 and ~360 m (layers g, h, and i in Fig. 2B). Interestingly, layer g shows different reflection texture compared with layers f and h. The reflection wave is comparable to those of bedded rocks—e.g., sedimentary or pyroclastic rocks on Earth. Considering the geological history of the lunar mare area (*15*), we propose that this layer is probably bedded or interlayered lava flow and/or pyroclastic rocks or thin and multilayered basaltic lavas.

Current regional geologic studies suggest that at least five episodes of lava eruptions filled the northeast region of the Imbrium basin, forming about 1-km-thick basaltic layers (*16*). Yutu's LPR has revealed five distinct episodes of pyroclastic/lava filling events within the upper ~400 m depth, although it is very likely that more episodes of volcanic eruptions have filled the Imbrium basin at greater depths (*8*).

Integrated geologic and geophysical explorations using the scientific payloads onboard the Yutu rover have revealed the detailed subsurface geological structures and the geological history of this area. Compared with previous Apollo and Luna landing sites, this area has the youngest mare basalts that appear to have unusual petrofabric characteristics. The LPR data have revealed complex subsurface structures of shallow crust within the mare, providing valuable information to reveal the lava eruption extents, style, and filling history within the Imbrium basin and the production history of regolith since ~3.3 Ga (Fig. 3). The available data suggest that the diversity of geological characteristics and thermal history of different lunar mare areas indicates there is more complex geological history than we had thought.

REFERENCES AND NOTES

1. L. Xiao, *Nat. Geosci.* **7**, 391–392 (2014).
2. Materials and methods are available as supplementary materials on *Science* Online.
3. H. Hiesinger, J. Head, U. Wolf, R. Jaumann, G. Neukum, *Spec. Pap. Geol. Soc. Am.* **477**, 1–51 (2011).
4. G. G. Schaber, G. A. Swann, *Proc. Lunar Planet. Sci. Conf.* **1**, 27–38 (1971).
5. E. W. Wolfe, N. G. Bailey, *Proc. Lunar Planet. Sci. Conf.* **1**, 15–25 (1972).
6. T. H. Prettyman *et al.*, *J. Geophys. Res.* **111** (E12), E12007 (2006).
7. E. M. Shoemaker *et al.*, *J. Geophys. Res.* **74**, 6081–6119 (1969).
8. F. Thiessen, S. Besse, M. I. Staid, H. Hiesinger, *Planet. Space Sci.* **104**, 244–252 (2014).
9. G. Y. Fang *et al.*, *Research in Astronomy and Astrophysics* **14**, 1607–1622 (2014).
10. N. Zhao, P. Zhu, K. Yang, Y. Yuan, S. Guo, *Sci. China-Phys. Mech. Astron.* **57**, 2346–2353 (2014).
11. J. Zhao *et al.*, *Sci. China-Phys. Mech. Astron.* **57**, 569–576 (2014).
12. T. R. McGetchin, M. Settle, J. Head, *Earth Planet. Sci. Lett.* **20**, 226–236 (1973).
13. B. B. Wilcox, M. S. Robinson, P. C. Thomas, B. R. Hawke, *Meteorit. Planet. Sci.* **40**, 695–710 (2005).
14. L. Qiao, L. Xiao, J. Zhao, Q. Huang, J. Haruyama, *Planet. Space Sci.* **101**, 37–52 (2014).
15. B. L. Jolliff, M. A. Wieczorek, C. K. Shearer, C. R. Neal, Eds., *New Views of the Moon* (Mineralogical Society of America, Chantilly, VA, 2006).
16. B. J. Thomson, E. B. Grosfils, D. B. J. Bussey, P. D. Spudis, *Geophys. Res. Lett.* **36**, L12201 (2009).
17. Z. Wang, Y. Li, J. Jiang, D. Li, *Sci. China Earth Sci.* **53**, 1365–1378 (2010).

ACKNOWLEDGMENTS

All the authors acknowledge support from the Key Research Program of the Chinese Academy of Sciences (grant KGZD-EW-603). L.X., Z.Y.X., J.N.Z., L.Q., and J.H. acknowledge support of the Natural Science Foundation of China (grant 41373066). X.P.Z. acknowledges support from the Science and Technology Development Fund (FDCT) of Macau (grants 068/2011/A, 048/2012/A2, and 091/2013/A3). We thank C. L. Li and the Ground Application System of Lunar Exploration, National Astronomical Observatories, Chinese Academy of Sciences, for their valuable and efficient help on data calibration and supplying. Author contributions: L.X., Z.Y.X., J.N.Z., L.Q., Y.L.Z., J.H., H.Z., X.P.Z., J.W., Q. Huang, and Q. He processed the imagery data and conducted image and radar data interpretation and geological analysis. P.M.Z., G.Y.F., N.Z., and Y.F.Y processed LPR data and did interpretation. B.Z, Y.C.J., Q.Y.Z., S.X.S., Y.X.L., and Y.Z.G. are team members of the LPR instrument. All authors contributed to the writing of the paper. The imagery data obtained by the Panoramic Camera onboard Yutu are the level 2C data. The imagery data obtained by the Descent Camera onboard the Chang'E-3 lander are the level 2A data. The IDs for the images used in the figures are listed in table S2 in the supplementary materials. Data presented in this paper are hosted at http://moon.bao.ac.cn.

SUPPLEMENTARY MATERIALS

www.sciencemag.org/content/347/6227/1226/suppl/DC1
Materials and Methods
Figs. S1 to S14
Tables S1 and S2
References (*18*–*30*)

11 August 2014; accepted 5 February 2015
10.1126/science.1259866

QUANTUM WALKS

Strongly correlated quantum walks in optical lattices

Philipp M. Preiss,[1] Ruichao Ma,[1] M. Eric Tai,[1] Alexander Lukin,[1] Matthew Rispoli,[1] Philip Zupancic,[1]* Yoav Lahini,[2] Rajibul Islam,[1] Markus Greiner[1]†

Full control over the dynamics of interacting, indistinguishable quantum particles is an important prerequisite for the experimental study of strongly correlated quantum matter and the implementation of high-fidelity quantum information processing. We demonstrate such control over the quantum walk—the quantum mechanical analog of the classical random walk—in the regime where dynamics are dominated by interparticle interactions. Using interacting bosonic atoms in an optical lattice, we directly observed fundamental effects such as the emergence of correlations in two-particle quantum walks, as well as strongly correlated Bloch oscillations in tilted optical lattices. Our approach can be scaled to larger systems, greatly extending the class of problems accessible via quantum walks.

Quantum walks are the quantum mechanical analogs of the classical random walk process, describing the propagation of quantum particles on periodic potentials (*1*, *2*). Unlike classical objects, particles performing a quantum walk can be in a superposition state and take all possible paths through their environment simultaneously, leading to faster propagation and enhanced sensitivity to initial conditions. These properties have generated considerable interest in using quantum walks for the study of position-space quantum dynamics and for quantum information processing (*3*). Two distinct models of quantum walk with similar physical behavior were devised: (i) the discrete-time quantum walk (*1*), in which the particle propagates in discrete steps determined by a dynamic internal degree of freedom, and (ii) the continuous-time quantum walk (*2*), in which the dynamics is described by a time-independent lattice Hamiltonian.

Experimentally, quantum walks have been implemented for photons (*4*), trapped ions (*5*, *6*), and neutral atoms (*7*–*9*), among other platforms (*4*). Until recently, most experiments were aimed at observing the quantum walks of a single quantum particle, which are described by classical wave equations.

[1]Department of Physics, Harvard University, Cambridge, MA 02138, USA. [2]Department of Physics, Massachusetts Institute of Technology, Cambridge, MA 02139, USA.
*Present address: Institute for Quantum Electronics, ETH Zürich, 8093 Zürich, Switzerland. †Corresponding author. E-mail: greiner@physics.harvard.edu